nature nanotechnology

LETTERS

PUBLISHED ONLINE: 2 SEPTEMBER 2012 | DOI: 10.1038/NNANO.2012.147

Probing the conductance superposition law in single-molecule circuits with parallel paths

H. Vazquez[1‡], R. Skouta[2‡], S. Schneebeli[2], M. Kamenetska[1†], R. Breslow[2*], L. Venkataraman[1*] and M.S. Hybertsen[3*]

According to Kirchhoff's circuit laws, the net conductance of two parallel components in an electronic circuit is the sum of the individual conductances. However, when the circuit dimensions are comparable to the electronic phase coherence length, quantum interference effects play a critical role[1], as exemplified by the Aharonov–Bohm effect in metal rings[2,3]. At the molecular scale, interference effects dramatically reduce the electron transfer rate through a meta-connected benzene ring when compared with a para-connected benzene ring[4,5]. For longer conjugated and cross-conjugated molecules, destructive interference effects have been observed in the tunnelling conductance through molecular junctions[6–10]. Here, we investigate the conductance superposition law for parallel components in single-molecule circuits, particularly the role of interference. We synthesize a series of molecular systems that contain either one backbone or two backbones in parallel, bonded together cofacially by a common linker on each end. Single-molecule conductance measurements and transport calculations based on density functional theory show that the conductance of a double-backbone molecular junction can be more than twice that of a single-backbone junction, providing clear evidence for constructive interference.

The simplest example in which conductance superposition might be investigated in nanoscale circuits is that of identical molecules bridging two electrodes. Indeed, theory suggests that the collective (interference) effects in arrays of molecules affect the net conductance of such a circuit, but the quantitative results are sensitive to details of junction structure[11–16]. However, the control of structure and a more precise probe of the conductance superposition law may be naturally achieved by building parallel molecular wire components into a single-molecular structure connected by local chemical bonds (Fig. 1a). An early analysis of this arrangement[12] provided an appealing result under idealized conditions in the regime of tunnelling conductance: the total conductance is the sum of the conductance of the individual branches plus an interference term $G_{tot} = G_1 + G_2 + 2\sqrt{G_1 G_2}$. Although numerical calculations showed that the quantitative value for the interference term could vary from this ideal expression[12], molecules with parallel backbone structures (Fig. 1a) are good candidates for observing a clear experimental signature of constructive interference effects in molecular-scale junctions.

Accordingly, we designed and synthesized a series of molecular systems consisting of two types of structures. The first, exemplified by 1,4-bis(methyl(thio)methyl)–benzene (**1**), has a single backbone that consists of a CH_2–benzene–CH_2 unit with methyl-sulphide linkers[17] (Fig. 1b, top panel). The second is 2,11-dithia(3,3)paracyclophane (**2**). It has two such CH_2–benzene–CH_2 units connected to common sulphur atoms at each end, as illustrated in Fig. 1b (lower panel). In both cases, the terminal sulphur groups bind to the gold leads through donor–acceptor bonds to undercoordinated sites[17,18]. A total of four pairs of molecules, including derivatives of **1** and **2**, were synthesized (for methods see Supplementary Section S1).

The characteristic signatures of constructive interference in the conductance of a double-backbone circuit formed from **2** emerge from a simple model for the electron transmission spectra. The frontier orbitals that couple and form the single-molecule circuit are illustrated in Fig. 1c for **2** (see Supplementary Section S4 for details of the analysis). The backbone orbitals are essentially bonding and antibonding combinations of the frontier molecular orbitals, for example, the lowest unoccupied molecular orbital (LUMO) of the single-backbone species **1**. In the ideal case, where the backbones are equivalent and degenerate, only the bonding combination has electronic coupling to the gateway states (the states on the sulphur–gold links to the electrodes). This coupling is $\sqrt{2}$ larger than the coupling in the single-backbone species (τ) and it encodes the interference effect in the junction. With the electrode Fermi level approximately in the middle of the molecular gap, characteristic of tunnelling conductance scenarios, the electron transmission is easily calculated for this model for **2** and for the analogous model for **1**. A Green's function approach is used under the additional assumption of an energy-independent transfer rate Γ coupling the gateway states to the bulk electrodes. From a comparison of the model transmission spectra for **1** and **2** (Fig. 1d), two characteristic features of interference emerge. First, the low bias conductance from transmission at the Fermi energy ($G = G_0 \times T(E_F)$, $G_0 = 2e^2/h$) for the double-backbone species is more than double that for the single-backbone species. The specific value of the conductance ratio $G(\mathbf{2})/G(\mathbf{1})$ depends on the details, but in the most idealized limit (degenerate backbone levels with small through space coupling, vanishing τ, large and energy-independent Γ and E_F at midgap), the ratio is four, as found previously[12]. Second, the width of the LUMO-derived transmission resonance for **2** is twice that of **1**.

We measured the conductance of the molecular junctions using the scanning tunnelling microscope (STM)-based break junction technique[19] (see Methods and Supplementary Section S3). Conductance (current/voltage) was repeatedly measured as a function of tip–sample displacement to generate conductance versus displacement traces. Figure 2a compares sample conductance traces from three molecules: **1** (green), **2** (black) and **1a** (red), which is an electronic analogue of **1** that is mechanically constrained,

[1]Department of Applied Physics and Applied Mathematics, Columbia University, 500 W. 120th Street, New York, New York 10027, USA, [2]Department of Chemistry, Columbia University, 3000 Broadway, New York 10027, USA, [3]Center for Functional Nanomaterials, Brookhaven National Laboratory, Upton, New York 11973, USA; [†]Present address: Department of Molecular Biophysics & Biochemistry and the Department of Physics, Yale University; [‡]These authors contributed equally to this work. *e-mail: rb33@columbia.edu; lv2117@columbia.edu; mhyberts@bnl.gov

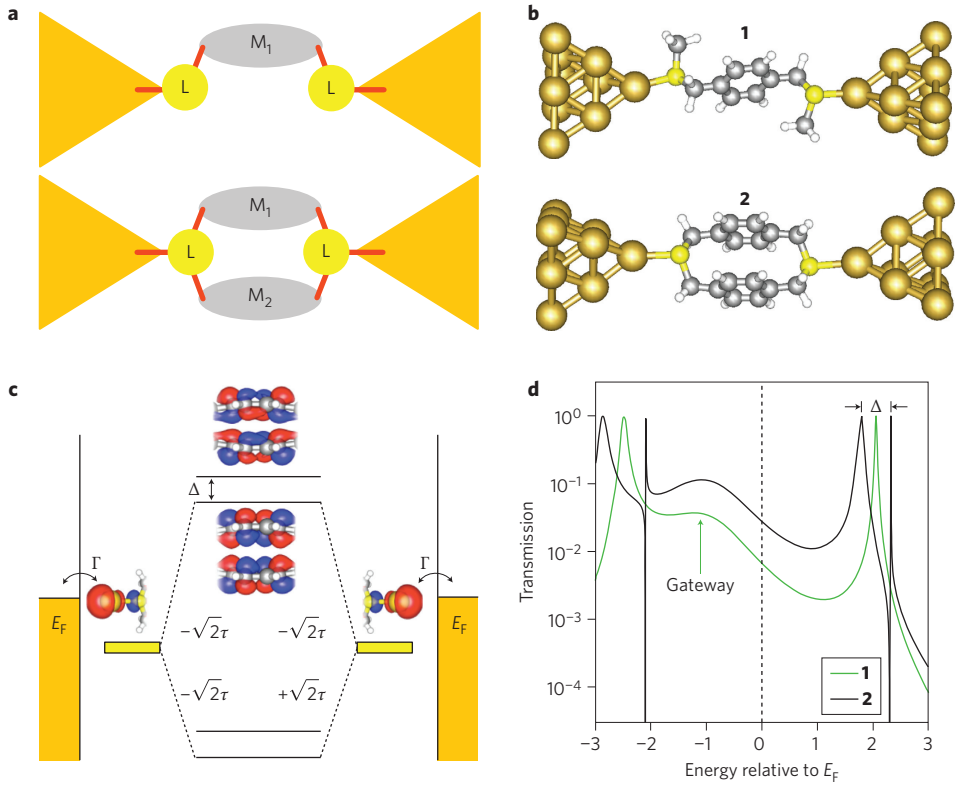

Figure 1 | Single-molecule circuits containing one and two conducting backbones connected in parallel. a, Schematic representation of circuits with one (top) and two (bottom) molecular backbones (M) connected in parallel through common links L. **b**, Chemical structure of exemplary molecules with single- (**1**) and double- (**2**) backbone molecules as studied in this work, visualized with a selective donor–acceptor bond between the sulphur link atom and idealized pyramidal gold tips. **c**, Model and schematic energy level diagram for the double-backbone junction formed from **2**. Through-space coupling results in the formation of bonding (bottom contour plot) and antibonding (top contour plot) combinations of the lowest empty backbone states, which split by an energy Δ. Only the bonding combination couples through bond to the suphur–gold gateway states on the links ($\sqrt{2}\tau$). Electrons on the gateway states are approximately resonant with the Fermi energy (E_F) of the metal electrodes and escape to the electrodes with rate Γ. Highest occupied backbone state energy levels are also indicated. **d**, Model transmission spectra for a single- (green) and double- (black) backbone circuit showing the contribution from each backbone state and the gateway states. The antibonding combinations of the backbone energy levels appear as dispersive peaks split by Δ from the dominant bonding combination because the degeneracy was slightly broken to provide weak coupling to them. The model Hamiltonian and the numerical parameters used are given in Supplementary Section S4.

like **2**. **1a** is a two-backbone molecule with one side conjugated (CH_2–benzene–CH_2) and the other saturated (C_4H_8). We see conductance features at integer multiples of G_0, as well as features below G_0 at molecule-specific values. The measured data from more than 6,000 independent traces for each molecule, without data selection, were used to form histograms that represent the conductance characteristics of a statistically significant ensemble of junctions (for details see Supplementary Section S3). These are shown in Fig. 2b on a linear scale. We see a low conductance peak for all three molecules, and also a higher conductance feature, similar to that observed in measurements of 4,4′-bipyridine[20,21]. Lorentzian fits to the low conductance peak are also shown in Fig. 2b. We find the most probable conductances (peak of the Lorentzian fit) to be $3.3 \times 10^{-4}G_0$, $2.9 \times 10^{-4}G_0$ and $9.0 \times 10^{-4}G_0$ for **1**, **1a** and **2**, respectively, giving a conductance ratio of $G(\mathbf{2})/G(\mathbf{1}) \approx 3$.

Because we see a broad, higher conductance feature in addition to the low conductance peak, we created two-dimensional conductance–displacement histograms to better understand the evolution of conductance with junction elongation[20,22]. Figure 2c–e presents two-dimensional conductance–displacement histograms for molecules **1**, **1a** and **2**, respectively. All molecules exhibit conductance features starting at $\sim 10^{-2}G_0$, immediately after the gold–gold contact is broken. Upon elongation, the junction conductance decreases for all molecules until a fully extended junction is formed, at a displacement of ~0.5–0.55 nm, just before the junction ruptures. Previous measurements with pyridine-terminated molecules have shown that broad, sloped conductance features that follow the gold–gold rupture result from enhanced gold–molecule coupling through a direct interaction between the π-system and the electrode[20,21]. The inter-electrode separation is smaller than the molecular backbone length, constraining the junction structure. The junction just before rupture (at ~0.5 nm elongation), on the other hand, consists of a molecule trapped between the tip and substrate in a fully extended configuration[20,21]. In this junction geometry, electronic coupling between the electrodes and the molecule is solely through the sulphur–gold link bond, as visualized in Fig. 1b, and representative of the conditions for the conductance superposition law under investigation. This portion of the data also corresponds to the low conductance peaks in Fig. 2b.

To isolate the data from fully extended junctions, we determined the conductance from a profile of the two-dimensional histograms, as shown in Fig. 2f. These profiles integrate all counts within a 0.1 nm window demarcated by the lines in Fig. 2c–e at an extension of ~0.5 nm, chosen to capture the final junction conductance. At this extension, the conductance of **1** peaks at $3.5 \times 10^{-4}G_0$, the conductance of **1a** at $2.8 \times 10^{-4}G_0$ and the conductance of **2** at $9.7 \times 10^{-4}G_0$. The conductance of **1** determined both from the one- and two-dimensional histograms is slightly higher than that of **1a**, indicating that the additional flexibility of **1** when compared

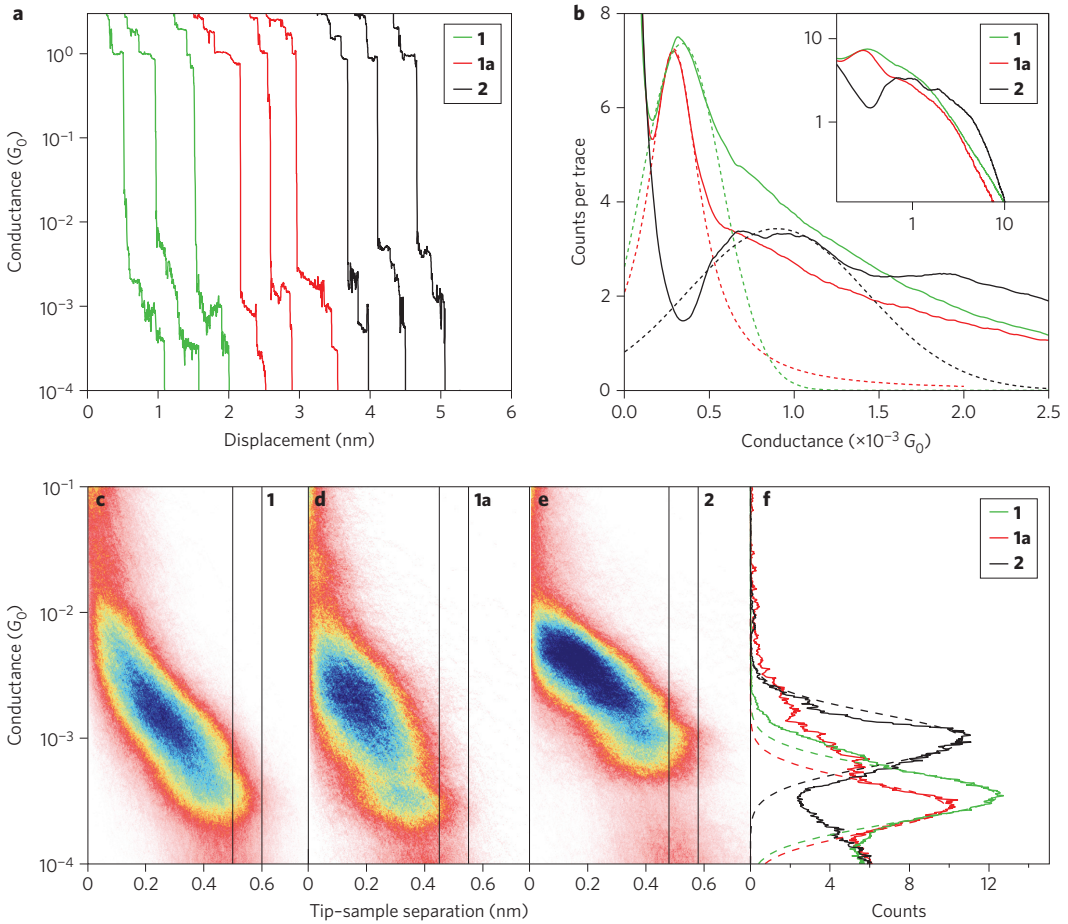

Figure 2 | STM break-junction measurements of single-molecule conductance. a, Sample traces showing conductance as a function of relative tip–sample displacement for molecules **1**, **1a** and **2** (the structure of **1a** is shown in Supplementary Fig. S6). **b**, Conductance histograms (on a linear scale) representing data from more than 6,000 traces for each molecule: **1**, **1a** and **2**. Dashed lines indicate Lorentzian fits to the peaks. Inset: same data on a log scale. **c**–**e**, Two-dimensional conductance–displacement histograms for junctions with molecules **1** (**c**), **1a** (**d**) and **2** (**e**). The relative tip–substrate displacement is set to zero where the gold–gold contact ruptures, and data beyond this rupture are plotted here using logarithmic bins along the conductance axis and linear bins along the displacement axis. **f**, Conductance profile determined from two-dimensional histograms for **1**, **1a** and **2** over a width of 0.1 nm centred at the end of the low-conductance feature (~0.5 nm displacement) and shown by the vertical lines in **c**,**d** and **e**, respectively. Dashed lines indicate Gaussian fits to the peaks.

with **1a** enables the formation of junctions that have a higher conductance. Nonetheless, the mechanical constraints in **1a** play a minor role in the measured conductance and, for the rest of this Letter, we will restrict our comparison to **1** and **2**, which form a pair of molecules with a conductance ratio $G(\mathbf{2})/G(\mathbf{1}) = 2.8$, evidence of the effects of constructive quantum interference.

Extensive density functional theory (DFT) studies of junction transmission (see Methods and Supplementary Section S4) were carried out for representative structures to elucidate the impact of a realistic molecule electronic structure on interference characteristics. To eliminate the role of junction structure in a comparison of **1** and **2**, we began with a model compound **1c**, obtained by cutting one backbone out of compound **2** and saturating the cut bonds with hydrogen atoms (Supplementary Fig. S5C). The calculated transmission spectra of **1c** and **2** are presented in Fig. 3a, and a visualization of the scattering states in the junction at selected energies is shown in Fig. 3b,c. In the unoccupied part of the spectrum, **2** exhibits twice as many peaks as **1c**. The LUMO-derived π-resonance at 2.1 eV for **1c** results in a bonding (LUMO at 1.9 eV) and an antibonding (LUMO + 2 at 2.5 eV) combination in **2**. The bonding peak of **2** is 1.8 times broader than the peak of **1c**, showing the second characteristic signature of interference. Similarly, the LUMO + 1 derived peak of **1c** at 2.5 eV gives rise to two peaks for **2** (LUMO + 1 and LUMO + 3, shown in Supplementary Fig. S7B); the anti-bonding peak at 3 eV shows dispersive character, as shown in the model (Fig. 1d). On the occupied side, the single peaks at −1.7 eV in each spectrum do not represent backbone peaks; rather, they arise from the gold–sulphur bonds (the gateway states in the simplified model) and decay across the backbones (Fig. 3b,c). This peak due to the gateway states is sharper than suggested by the simple model in Fig. 1d. A detailed analysis of the scattering states over several electronvolts around E_F shows that the character of the states on the gold–sulphur link atoms changes with energy, modulating the coupling to the electrodes and illustrating the complexity of the full electronic structure.

The Fermi energy falls between the gateway state resonance and the backbone LUMO resonance. The low bias conductance for all molecules is dominated by one transmission channel. In each case, the scattering state at E_F responsible for low bias conductance (Fig. 3b,c) clearly shows tunnelling character. The atomic character of the gold–sulphur link atoms is similar to the gateway resonance, whereas the through-π-bond portion on the backbones exhibits a nodal pattern that is approaching that of the LUMO peak, which is closest to E_F. For the double-backbone case, the transmission channel is clearly derived only from the bonding combination of π backbone states, the signature of constructive interference.

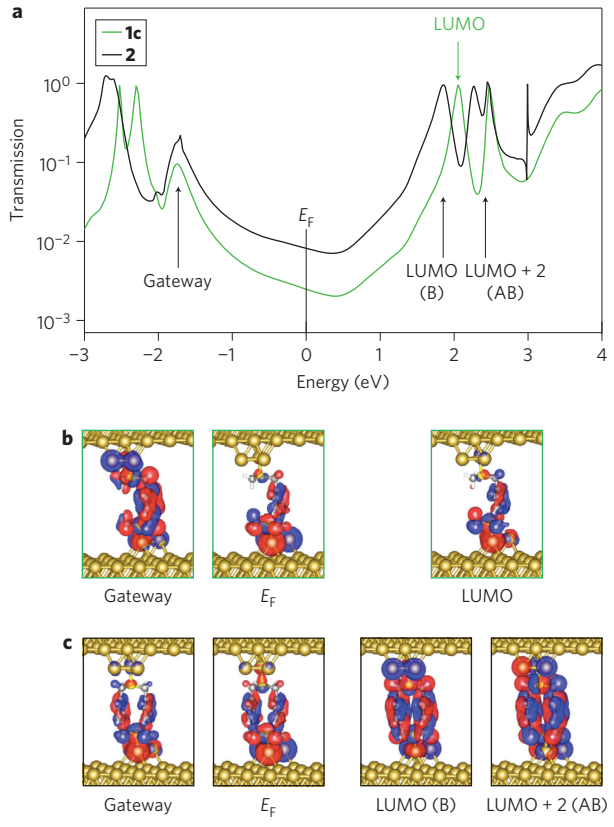

Figure 3 | Calculated transmission properties comparing a double-backbone circuit with an idealized, single-backbone circuit. a, Transmission spectra of the 'cut' molecule **1c** (green) and of **2** (black) bound to gold electrodes. The gold–sulphur gateway states, the electrode Fermi energy, the LUMO of **1c** and its corresponding bonding and antibonding pair in **2** (LUMO and LUMO + 2) are marked. **b**,**c**, Contour plots of the real part of the calculated scattering states of **1c** and **2** at these energies are shown for **1c** (**b**) and **2** (**c**). The bonding versus antibonding character for the LUMO-derived resonances is seen in the nodal pattern in **c**.

The calculated conductances for **1c** and **2** are $2.5 \times 10^{-3} G_0$ and $8.2 \times 10^{-3} G_0$, giving a ratio of $G(\mathbf{2})/G(\mathbf{1c}) = 3.3$. These DFT-based conductance values are larger than the measured values, as is often seen due to the inherent errors in DFT-based transport calculations[23–25]. Correcting for these errors[23] does not change the calculated conductance ratio by more than 20% (see Supplementary Section S4). Calculations for the measured molecules **1** and **1a** show, qualitatively, the same transmission spectra as **1c** (Supplementary Figs S5D and S6). The calculated conductance values are slightly higher than that of **1c** (Supplementary Table S2). To further explore the impact of junction geometry, we considered an alternative gold tip structure (Supplementary Table S2) and the effect of elongating the junction relative to the minimum energy junction geometry (Supplementary Fig. S10). Overall, due to plausible geometry and local junction structure changes, the variation in the calculated conductance values falls within the width of the measured histograms, as seen in the analysis of other junctions[23], and the results for the calculated conductance ratios are robust.

The analysis so far suggests that the conductance ratio may be sensitive to the interplay between the placement of the Fermi energy, the energies of the link states and the placement of the backbone resonances. To probe this further, we synthesized two additional derivatives of both molecules **1** and **2**, with fluorine (F) or methoxy (OMe) substituents on the benzene rings (**1F**, **2F**, **1OMe** and **2OMe**, respectively) and a single- and double-backbone fluorene derivative (**1Fl** and **2Fl**) (see Table 1 for structures). Two-dimensional conductance histograms for these compounds are qualitatively similar to the histograms for **1** and **2** (Supplementary Figs S1–S3). The measured ratio of the conductances of the double- and single-backbone molecules for the substituted benzenes is slightly larger than 2 for both the fluorine- and OMe-substituent backbones and close to 2 for the fluorene backbones (Table 1). The calculated transmission spectra are qualitatively similar (Supplementary Figs S8, S9) and they demonstrate the increase in the width of the LUMO transmission peak characteristic of coherent linear combinations of both backbone states—the interference effect. The calculated conductance ratios follow the measured trends and reveal one of the systematic differences between these double-backbone molecules when compared to **2**. For **2**, the HOMO-derived transmission resonances appear at an energy below the gold–sulphur gateway resonances (−1.7 eV in Fig. 3a). The substituents raise the HOMO-derived states such that (antibonding) resonances in the double-backbone molecules fall in the energy window of the gold–sulphur gateway states, reducing transmission for energies below E_F and decreasing the conductance ratio for these substituted pairs.

Table 1 | Calculated and measured single-molecule conductance for pairs of molecules with a single backbone and two such backbones in parallel and also the ratio between the conductance of the double-backbone molecule and its single-backbone analogue.

Molecule	Backbone structure	Calculated conductance, G_0	Calculated ratio, $G(2)/G(1)$	Measured conductance, G_0	Measured ratio, $G(2)/G(1)$
1 **2**	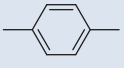	2.7×10^{-3} 8.2×10^{-3}	3.0	3.5×10^{-4} 9.7×10^{-4}	2.8
1F **2F**	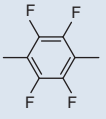	3.5×10^{-3} 4.8×10^{-3}	1.4	3.1×10^{-4} 6.5×10^{-4}	2.1
1OMe **2OMe**	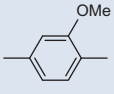	2.0×10^{-3} 6.2×10^{-3}	2.4	3.5×10^{-4} 8.7×10^{-4}	2.5
1Fl **2Fl**	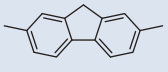	7.2×10^{-4} 13.0×10^{-4}	1.8	1.1×10^{-4} 1.8×10^{-4}	1.6

In summary, we have probed the conductance superposition law in single-molecule junctions by combining chemical synthesis, single-molecule measurements and transport calculations. Constructive quantum interference in molecules with two parallel backbones is observed to lead to a characteristic conductance that is more than twice that of a molecule with a single backbone. Transport calculations also show a characteristic broadening of the primary transmission resonances for the double-backbone case and indicate that the electronic structure of the linker group plays a subtle but important quantitative role in determining the conductance value. Our experiments and calculations illustrate some of the complexity involved in teasing out clear signatures of interference effects in single-molecule junctions.

Methods

Experiments. Single-molecule junctions were created by repeatedly forming and breaking a gold point contact in a solution of the target molecules in 1,2,4-trichlorobenzene under 350 mV bias with a velocity of 15 nm s^{-1} in a home-built STM[26]. Thousands of traces were collected and presented as conductance histograms, with the peaks corresponding to the most frequently observed conductance values. A freshly cut gold wire (diameter, 0.25 mm; 99.999% purity, Alfa Aesar) was used as the tip, and an ultraviolet/ozone-cleaned gold substrate (mica with 100 nm gold, 99.999% purity, Alfa Aesar) was used as the substrate. The STM operated under ambient conditions at room temperature. To ensure that each measurement started from a different initial atomic configuration of the electrodes, the electrodes were pulled apart only after being brought into contact with the gold surface, indicated by a conductance greater than a few G_0. Before adding a molecular solution between the tip and substrate, 1,000 conductance traces were first collected without molecules to ensure that there were no contaminations in the STM set-up. Further details are provided in Supplementary Section S3.

Calculations. DFT-based first-principles calculations of electronic transmission[27,28] were carried out with a gradient-corrected exchange-correlation functional[29] and a non-equilibrium Green's function approach. Junction structures all corresponded to local energy minima. The real part of the scattering states, calculated for surface $k = 0$, were presented for analysis[30]. Further details are presented in Supplementary Section S4.

Received 16 May 2012; accepted 27 July 2012;
published online 2 September 2012

References

1. Beenakker, C. W. J. & van Houten, H. Quantum transport in semiconductor nanostructures. *Solid State Phys.* **44,** 1–228 (1991).
2. Aharonov, Y. & Bohm, D. Significance of electromagnetic potentials in the quantum theory. *Phys. Rev.* **115,** 485–491 (1959).
3. Webb, R. A., Washburn, S., Umbach, C. P. & Laibowitz, R. B. Observation of h/e Aharonov–Bohm oscillations in normal-metal rings. *Phys. Rev. Lett.* **54,** 2696–2699 (1985).
4. Sautet, P. & Joachim, C. Electronic interference produced by a benzene embedded in a polyacetylene chain. *Chem. Phys. Lett.* **153,** 511–516 (1988).
5. Patoux, C., Coudret, C., Launay, J-P., Joachim, C. & Gourdon, A. Topological effects on intramolecular electron transfer via quantum interference. *Inorg. Chem.* **36,** 5037–5049 (1997).
6. Mayor, M. *et al.* Electric current through a molecular rod—relevance of the position of the anchor groups. *Angew. Chem. Int. Ed.* **42,** 5834–5838 (2003).
7. Kiguchi, M., Nakamura, H., Takahashi, Y., Takahashi, T. & Ohto, T. Effect of anchoring group position on formation and conductance of a single disubstituted benzene molecule bridging Au electrodes: change of conductive molecular orbital and electron pathway. *J. Phys. Chem. C* **114,** 22254–22261 (2010).
8. Fracasso, D., Valkenier, H., Hummelen, J. C., Solomon, G. C. & Chiechi, R. C. Evidence for quantum interference in SAMs of arylethynylene thiolates in tunneling junctions with eutectic Ga–In (EGaIn) top-contacts. *J. Am. Chem. Soc.* **133,** 9556–9563 (2011).
9. Guedon, C. M. *et al.* Observation of quantum interference in molecular charge transport. *Nature Nanotech.* **7,** 305–309 (2012).
10. Aradhya, S. V. *et al.* Dissecting contact mechanics from quantum interference in single-molecule junctions of stilbene derivatives. *Nano Lett.* **12,** 1643–1647 (2012).
11. Yaliraki, S. N. & Ratner, M. A. Molecule–interface coupling effects on electronic transport in molecular wires. *J. Chem. Phys.* **109,** 5036–5043 (1998).
12. Magoga, M. & Joachim, C. Conductance of molecular wires connected or bonded in parallel. *Phys. Rev. B* **59,** 16011–16021 (1999).
13. Lang, N. D. & Avouris, P. Electrical conductance of parallel atomic wires. *Phys. Rev. B* **62,** 7325–7329 (2000).
14. Liu, R., Ke, S-H., Baranger, H. U. & Yang, W. Intermolecular effect in molecular electronics. *J. Chem. Phys.* **122,** 044703 (2005).
15. Landau, A., Kronik, L. & Nitzan, A. Cooperative effects in molecular conduction. *J. Comput. Theor. Nanosci.* **5,** 535–544 (2008).
16. Reuter, M. G., Seideman, T. & Ratner, M. A. Molecular conduction through adlayers: cooperative effects can help or hamper electron transport. *Nano Lett.* **11,** 4693–4696 (2011).
17. Park, Y. S. *et al.* Contact chemistry and single-molecule conductance: a comparison of phosphines, methyl sulfides, and amines. *J. Am. Chem. Soc.* **129,** 15768–15769 (2007).
18. Park, Y. S. *et al.* Frustrated rotations in single-molecule junctions. *J. Am. Chem. Soc.* **131,** 10820–10821 (2009).
19. Xu, B. Q. & Tao, N. J. Measurement of single-molecule resistance by repeated formation of molecular junctions. *Science* **301,** 1221–1223 (2003).
20. Quek, S. Y. *et al.* Mechanically controlled binary conductance switching of a single-molecule junction. *Nature Nanotech.* **4,** 230–234 (2009).
21. Kamenetska, M. *et al.* Conductance and geometry of pyridine-linked single-molecule junctions. *J. Am. Chem. Soc.* **132,** 6817–6821 (2010).
22. Martin, C. A. *et al.* Fullerene-based anchoring groups for molecular electronics. *J. Am. Chem. Soc.* **130,** 13198–13199 (2008).
23. Quek, S. Y. *et al.* Amine-gold linked single-molecule circuits: experiment and theory. *Nano Lett.* **7,** 3477–3482 (2007).
24. Quek, S. Y., Choi, H. J., Louie, S. G. & Neaton, J. B. Length dependence of conductance in aromatic single-molecule junctions. *Nano Lett.* **9,** 3949–3953 (2009).
25. Strange, M., Rostgaard, C., Hakkinen, H. & Thygesen, K. S. Self-consistent GW calculations of electronic transport in thiol- and amine-linked molecular junctions. *Phys. Rev. B* **83,** 115108 (2011).
26. Venkataraman, L. *et al.* Single-molecule circuits with well-defined molecular conductance. *Nano Lett.* **6,** 458–462 (2006).
27. Soler, J. M. *et al.* The SIESTA method for *ab initio* order-*N* materials simulation. *J. Phys. Condens. Matter* **14,** 2745–2779 (2002).
28. Brandbyge, M., Mozos, J. L., Ordejon, P., Taylor, J. & Stokbro, K. Density-functional method for nonequilibrium electron transport. *Phys. Rev. B* **65,** 165401 (2002).
29. Perdew, J. P., Burke, K. & Ernzerhof, M. Generalized gradient approximation made simple. *Phys. Rev. Lett.* **77,** 3865–3868 (1996).
30. Paulsson, M. & Brandbyge, M. Transmission eigenchannels from nonequilibrium Green's functions. *Phys. Rev. B* **76,** 115117 (2007).

Acknowledgements

This work was supported primarily by the Nanoscale Science and Engineering Initiative of the National Science Foundation (NSF, CHE-0641523), the New York State Office of Science, Technology, and Academic Research (NYSTAR) and an NSF Career Award to L.V. (CHE-07-44185). L.V. also thanks the Packard Foundation for support. This work was carried out in part at the Center for Functional Nanomaterials, Brookhaven National Laboratory, which is supported by the US Department of Energy, Office of Basic Energy Sciences (contract no. DE-AC02-98CH10886). R.S. acknowledges financial support from the Canadian postdoctoral fellowship FQRNT programme. S.T.S. acknowledges support from an Arun Guthikonda Memorial graduate fellowship. The authors thank the NSF (CHE-0619638) for the acquisition of an X-ray diffractometer, and G. Parkin and W. Sattler for obtaining our crystal structures.

Author contributions

The experiments were conceived by R.S., S.S., M.K., R.B. and L.V. Theory and calculations were conceived by H.V. and M.S.H. Synthesis and chemical analysis were performed by R.S. and S.S. Conductance measurements and analysis were performed by M.K and L.V. Calculations were performed by H.V. The manuscript was written by H.V., L.V. and M.S.H., with comments and input from all other authors.

Additional information

Supplementary information is available in the online version of the paper. Reprints and permission information is available online at http://www.nature.com/reprints. Correspondence and requests for materials should be addressed to R.B., L.V. and M.S.H.

Competing financial interests

The authors declare no competing financial interests.